A RADIOMETRIC CALIBRATION PROCEDURE FOR OPTICAL HARDWARE-IN-THE-LOOP STIMULATORS

Fabio Ornati[1*], Paolo Panicucci[1], Andrea Pizzetti[1], and Francesco Topputo[1].
[1]Politecnico di Milano, Department of Aerospace Science and Technology, Via La Masa 34, Milan, 10156, Italy
[*][fabio.ornati@polimi.it]

Abstract. *Optical stimulator facilities are viable and effective solution for testing optical navigation software and hardware. With these, the visual conditions met by navigation cameras in their operative scenarios can be emulated on ground to assess performance and validate the integrated system. This work introduces a novel radiometric calibration procedure to enable absolute and relative reproduction of radiometrically accurate space scenes in optical Hardware-In-the-Loop testbeds. The method is adaptable to both pointwise objects and resolved objects. The procedure is validated in end-to-end tests against both rendered scenarios and real night-sky images.*

Introduction. Increasing the autonomy of spacecraft systems is one of the key aspects for reducing the operational costs of future missions. Nowadays, important tasks such as navigation are still performed and supervised by ground personnel. This aspect, coupled with the limited availability of communication slots, limits the number of missions that can be operated simultaneously. With this regard, Vision-Based Navigation (VBN) techniques established themselves as one of the most viable technologies for achieving fully autonomous capabilities. Indeed these are able to provide accurate navigation solutions using reliable and lightweight optical sensors.

Validation and Verification (V&V) of VBN algorithms is a crucial aspect of their development process. During this phase, labeled datasets of space scene images are required to evaluate the performance and robustness of the algorithms. However, real datasets are limited in number as they cover only the trajectories flown by previous missions and are characterized by ground-truth errors. For these reasons, synthetic images are widely used to perform an extensive validation of the algorithms.

The synthetic datasets can be generated either directly via software rendering or thanks to optical stimulator facilities. These kinds of optical Hardware-In-the-Loop (HIL) testbeds are able to emulate the visual conditions that would be met by the navigation cameras in orbit. Over the years, a number of such facilities have been developed and discussed in the literature.[1–4] All of their designs share two key components: a screen that displays pre-generated synthetic scenes and a lens system to achieve collimation. Two of these facilities, named TinyV3RSE[5] and RETINA,[6] have been assembled at the Deep-Space Astrodynamics Research and Technology group (DART) and are currently supporting the development of optical navigation algorithms.[7,8] Indeed, optical stimulators are an effective solution for performing HIL simulations of the complete navigation apparatus. Among other advantages, the HIL technique allows investigating the interaction between the developed software and the real flight hardware. Different from software rendering, it is not required to accurately model the camera and sensor imaging behavior since all the hardware-related effects are intrinsically deriving from the hardware itself. This aspect is especially relevant when trying to reproduce particular effects such as diffraction, sensor saturation, and blooming, which are difficult to model accurately and may still have a strong impact upon the navigation algorithms.

In order to obtain realistic scenes, the optical stimulator facilities shall be accurately calibrated both geometrically and radiometrically. The geometric calibration ensures the precise reproduction of the geometric features. To obtain so, a mapping between the Line-of-Sight (LoS) directions sensed by the camera and those traced on the screen is characterized. The mapping allows the compensation of optical effects induced by the setup of the facility, such as distortions and misalignment between its components.[2,5] This work addresses radiometric calibration, which aims to faithfully reproduce the visual intensity of the features in the scenes.

Methodology. The radiometric calibration of an optical facility enables the conversion between a required value of radiometric intensity and the digital count of the pixels that shall be lighted on the stimulator screen.[1,4] In this work, such mapping is expressed in terms of flux density reaching the camera pupil. This quantity, being independent from the actual size of the pupil, allows the radiometric calibration procedure to be completely agnostic to the geometric characteristics of the camera under testing. The phases of the calibration procedures are schematized in Figure 1 and are described hereunder.

Facility characterization. In the initial step of the procedure, the screen response is characterized using real measurements. These are obtained through a high-accuracy light power meter. The sensor is used to sample the radiant flux density F at the location of the camera pupil generated by a group of screen pixels lit at a given digital count level B. Such measurements take into account both the different relative spectral distribution of the light produced by the screen and the spectral sensitivity of the power meter to achieve more accurate results. The output of this characterization is a curve $F(B)$ that relates the flux density with the digital count.

Spectral response scaling. The spectra of the screen and the one of the real objects that are reproduced in the HIL facility are generally quite different, both in extension and distribution. In fact, a screen produces light mostly distributed in the visible spectrum and characterized by

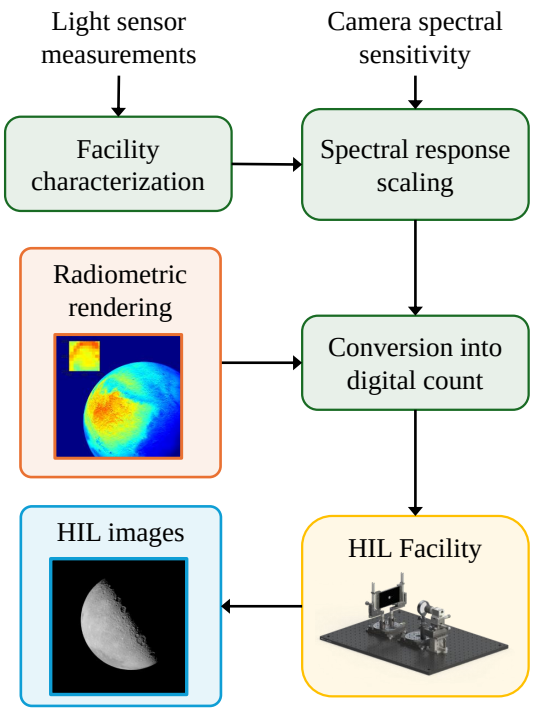

Figure 1. Workflow of radiometric calibration.

three peaks in correspondence of each color channel. On the other hand, the light reflected or emitted by an object in space would more closely resemble the one of a black emitter. This work provides a solution for achieving radiometric similarity by equating the effects that the two spectra would have on the camera that is being simulated in the facility. In practice, this is done by defining a new quantity called effective radiant flux density F_{eff} which is the radiant flux as weighted by the relative spectral response curve of the camera.

Rendering. The radiometric content of the simulated scenarios has to be known to emulate them in the facility. Therefore, a radiometrically consistent spectral rendering tool has to be used to generate the display scenes. These are no other than a discretized grid of angular directions, in which the value of each pixel represents the effective radiant flux density that would reach the pupil. If pointwise objects are reproduced, their magnitude is converted into a value F_{eff}, and a single pixel is lit. Finally, the value of the effective radiant flux density in each pixel is converted into an equivalent digital count by inverting the $F_{\text{eff}}(B)$ curve. The generated digital image can then be used in the facility to stimulate the camera.

Validation. The ability of the calibration procedure to replicate the radiometric properties is validated against both renderings and real night-sky images. In the first case, a scene is rendered twice, one time to generate a screen facility image and a second time considering the optical and radiometric characteristics of the real camera. The screen image is converted and acquired by the camera in the facility. A comparison is then made between the real photo and the rendered one. An example of this comparison is shown in Figure 2. This validation strategy is simple but it is not immune from rendering errors deriving from incorrect modeling of the camera characteristics. For this reason, the facility images are also compared against night sky photos, as shown in Figures 3 and 4. Note that night-sky images are attenuated by the atmosphere. On average, the ratio between the digital count of the real images and the one predicted by the renderer (and emulated in the facility) is close to 0.7.

Acknowledgments. This project has received funding from the European Research Council (ERC) under the European Union's Horizon 2020 research and innovation programme (grant agreement No. 864697).

References.

[1] G. Rufino and A. Moccia, "Laboratory test system for performance evaluation of advanced star sensors," *Journal of Guidance, Control, and Dynamics*, vol. 25, no. 2, pp. 200–208, 2002. DOI: 10.2514/2.4888.

[2] M. A. Samaan, S. R. Steffes, and S. Theil, "Star tracker real-time hardware in the loop testing using optical star simulator," *Spaceflight Mechanics*, vol. 140, 2011.

[3] N. Filipe, L. Jones-Wilson, S. Mohan, K. Lo, and W. Jones-Wilson, "Miniaturized star tracker stimulator for closed-loop testing of cubesats," *Journal of Guidance, Control, and Dynamics*, vol. 40, no. 12, pp. 3239–3246, 2017. DOI: 10.2514/1.G002794.

[4] C. Beierle and S. D'Amico, "Variable-magnification optical stimulator for training and validation of spaceborne vision-based navigation," *Journal of Spacecraft and Rockets*, vol. 56, no. 4, pp. 1060–1072, 2019. DOI: 10.2514/1.A34337.

[5] P. Panicucci and F. Topputo, "The tinyv3rse hardware-in-the-loop vision-based navigation facility," *Sensors*, vol. 22, no. 23, p. 9333, 2022. DOI: 10.3390/s22239333.

[6] F. Ornati, P. Panicucci, E. Andreis, and F. Topputo, "Retina: a highly-versatile optical facility for camera-in-the-loop testing of spaceborne vision-based sensors," in *46th AAS Guidance, Navigation and Control Conference*, pp. 1–19, 2024.

[7] E. Andreis, P. Panicucci, F. Ornati, and F. Topputo, "Towards validation and verification of autonomous vision-based navigation for interplanetary spacecraft," in *12th International Conference on Guidance, Navigation & Control Systems (GNC) and 9th International Conference on Astrodynamics Tools and Techniques (ICATT)*, pp. 1–14, 2023.

[8] P. Panicucci, F. Piccolo, A. Rizza, G. Merisio, F. Topputo, and R. Walker, "Vision-based navigation for the lumio cubesat mission," in *46th AAS Guidance, Navigation and Control Conference*, pp. 1–20, 2024.

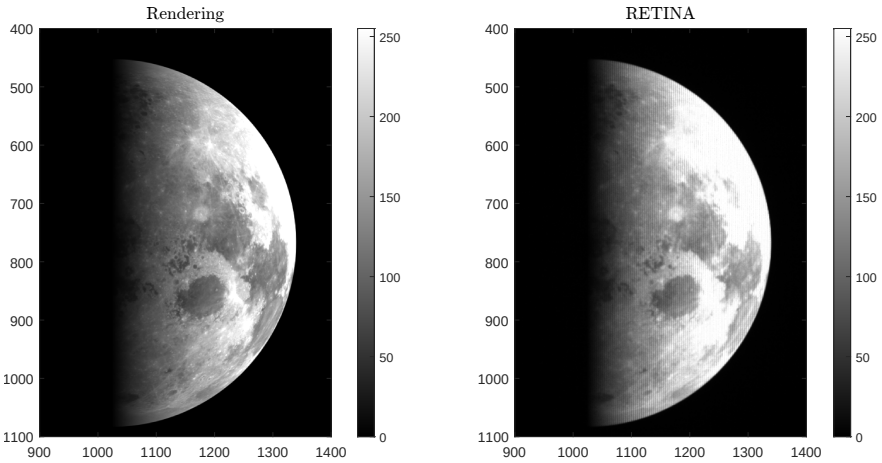

Figure 2. Comparison between a rendered image (center), and RETINA image (right) using the same camera.

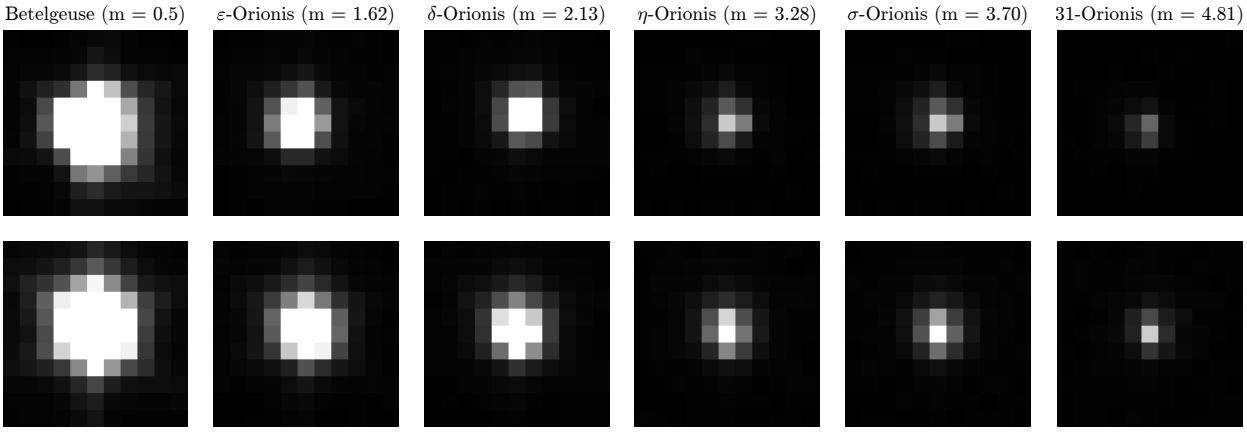

Figure 3. Comparison between unresolved objects in night-sky photos (top) and images acquired in the RETINA facility (bottom) using the same camera.

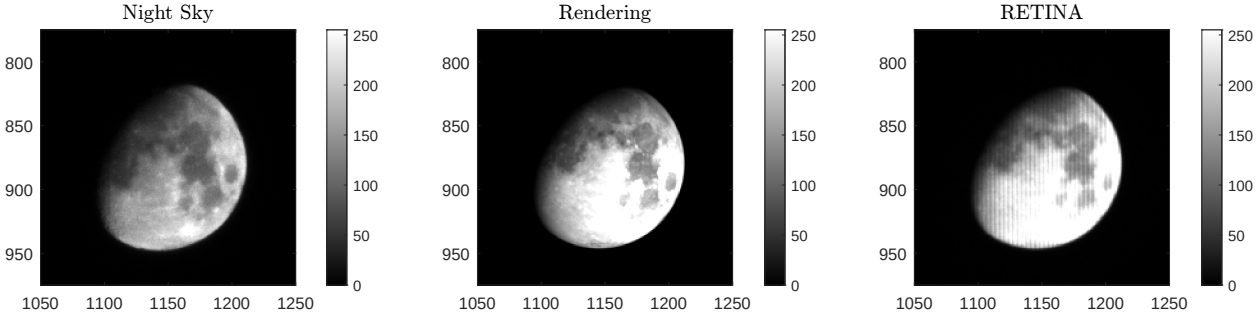

Figure 4. Comparison between moon night-sky image (left), software rendering (center), and RETINA image (right) using the same camera.